Mesoscale Phase Separation of Skyrmion-Vortex Matter in Chiral-Magnet–Superconductor Heterostructures

José F. Neto and Clécio C. de Souza Silva*
Departamento de Física, Universidade Federal de Pernambuco, Cidade Universitária, 50670-901 Recife-PE, Brazil

(Received 17 April 2021; revised 5 August 2021; accepted 6 January 2022; published 2 February 2022)

We investigate theoretically the equilibrium configurations of many magnetic skyrmions interacting with many superconducting vortices in a superconductor–chiral-magnet bilayer. We show that miscible mixtures of vortices and skyrmions in this system break down at a particular wave number for sufficiently strong coupling, giving place to remarkably diverse mesoscale patterns: gel, stripes, clusters, intercalated stripes, and composite gel-cluster structures. We also demonstrate that, by appropriate choice of parameters, one can thermally tune between the homogeneous and density-modulated phases.

DOI: 10.1103/PhysRevLett.128.057001

The combination of superconductivity and magnetism in hybrid magnet-superconductor materials has led to a remarkable range of novel phenomena and applications impossible to achieve when the constituent materials are taken isolatedly. Examples include dissipationless spin-polarized currents [1–3], spin valves with infinite magnetoresistance [4–6], a novel class of superconducting quantum devices [7–9], and controlled manipulation of flux quanta (Abrikosov vortices) in superconductors [10–19].

Recently, there has been increasing interest in the hybridization of topologically protected magnetic textures called skyrmions and Abrikosov vortices in heterostructures comprising a superconducting (SC) film and a chiral magnetic (CM) layer [20–26]. In these systems, a skyrmion and a nearby vortex interact with each other via their stray fields and/or via spin-orbit coupling (SOC) between the SC and CM layers. In the case of attractive interaction, they eventually form a bound pair with easily tunable dynamical properties [20–23,27]. In particular, for strong SOC, a skyrmion-vortex pair can host localized Majorana bound states, which makes SC-CM hybrids a promising platform for future applications in topological quantum computing [24,26,28,29].

The physics of many vortices and many skyrmions in SC-CM hybrids is still poorly understood. The ability of skyrmions to influence the vortex dynamics in the superconducting layer has recently been corroborated experimentally [25,26]. However, the impact of the vortex system in the magnetic state of the CM layer remains unknown. As it is often the case in the physics of many interacting objects, the composite many-skyrmion–many-vortex matter can exhibit new emergent properties not found when the skyrmion crystal and/or the vortex lattice are treated individually. Therefore, it is necessary to take into account the feedback of both subsystems on each other so as to investigate possible collective effects resulting from their mutual interaction.

In this Letter, we investigate equilibrium configurations of composite skyrmion-vortex matter in SC-CM heterostructures as a function of the main energy scales and characteristic lengths of the system. For weak skyrmion-vortex coupling, both vortices and skyrmions form homogeneous, quasitriangular lattices as a result of their repulsive intraspecies interaction. We show that, upon increasing the skyrmion-vortex coupling energy, the homogeneous distribution of vortices and skyrmions becomes unstable with respect to density fluctuations of a particular wavelength, irrespective of whether the skyrmion-vortex interaction is attractive or repulsive. This results in a series of density-modulated phases, such as clusters, stripes, and bubbles, similar to microphase separation phenomena observed in soft matter systems like block copolymers [30–32], colloidal suspensions [33,34], charged water-oil mixtures [35], and model systems with nonmonotonic interactions [36–40].

Model.—We consider a thin, chiral ferromagnetic film or multilayer of thickness d_M on top of a (SC) film of thickness d_S, both exposed to an off-plane, external magnetic field $\boldsymbol{B} = B\hat{\boldsymbol{z}}$ and separated by an insulating layer of thickness d_I (see Fig. 1). We assume that $d_S \ll \lambda$, where λ is the London penetration depth of the superconductor, so that the number of vortices is essentially given by $N_v \simeq A_{\mathrm{film}} B/\Phi_0$, where A_{film} is the film surface area. In addition, the skyrmions in the CM layer are assumed to coexist with a ferromagnetic background and $d_M \ll d_S$, so as to rule out the nucleation of vortices or vortex-antivortex pairs induced into the superconductor by the magnetic texture [21,22]. The number N_s of skyrmions in a CM layer can be controlled by a number of techniques, even for $B = 0$ [41–45]. Therefore, to cover a wide range of possibilities, we will change N_s and N_v independently. We further assume that vortex-vortex and skyrmion-skyrmion distances are considerably larger than their respective core

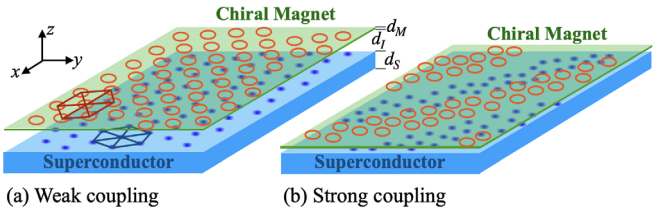

FIG. 1. Cartoon of the system geometry and illustration of possible distributions of skyrmions (rings) and vortices (dots) in two situations: (a) weak coupling between the SC and CM layers, where vortices and skyrmions form almost independent triangular lattices; (b) strong (repulsive) coupling, where the system self-organizes into a modulated phase.

sizes and that N_s and N_v are conserved, which is a good approximation for vortices in the thin film limit and for skyrmions when the CM layer is prepared in the skyrmion crystal phase [46].

With the considerations above, vortices and skyrmions can be treated as particles and their total free energy can be expressed as $\mathcal{F} = \mathcal{F}_0 + \mathcal{F}_{\rm int}$, where $\mathcal{F}_0$ is the self-energy of all vortices and skyrmions and $\mathcal{F}_{\rm int}$ is the superposition of all pair interactions, that is,

$$\mathcal{F}_{\rm int} = \frac{1}{2}\sum_{i,j=1}^{N_v} V_{vv}(r) + \frac{1}{2}\sum_{i,j=1}^{N_s} V_{ss}(r) + \sum_{i=1}^{N_v}\sum_{j=1}^{N_s} V_{vs}(r), \qquad (1)$$

where $r = |\boldsymbol{r}_i - \boldsymbol{r}_j|$, with $\boldsymbol{r}_i, \boldsymbol{r}_j$ as the positions of vortices or skyrmions in the xy plane. The vortex-vortex interaction is modeled by Pearl's potential, which can be expressed as $V_{vv}(r) = (\epsilon_{vv}/2\pi)\int d^2\boldsymbol{k} e^{i\boldsymbol{k}\cdot\boldsymbol{r}}/(k^2 + k/\Lambda)$, where $\Lambda = 2\lambda^2/d_s \gg \lambda$ is the Pearl length, $\epsilon_{vv} = \phi_0^2/\pi\mu_0\Lambda$, and $\phi_0 = h/2e$ is the flux quantum [52]. This is a long range repulsive potential, which for $r \ll \Lambda$ can be approximated by $\epsilon_{vv}\ln(\Lambda/r)$. For the skyrmion-skyrmion interaction, we use a modified Bessel function, which reflects the short range repulsive character of the potential for distances larger than the skyrmion radius $R_{\rm sk}$ [53–56]: $V_{ss}(r) = \epsilon_{ss}K_0(r/\xi_s)$, where ξ_s is the healing length of the spins outside the skyrmion core and ϵ_{ss} has been recently estimated as $\epsilon_{ss} \sim 60Ad_M(R_{\rm sk}/\xi_s)^4$ [56], with A as the exchange stiffness. Finally, we model the electromagnetic coupling between a vortex and a skyrmion by $V_{vs}(r) = \epsilon_{vs}/(1 + r^2/\lambda_{vs}^2)^2$, where ϵ_{vs} can be either negative or positive, depending on whether the skyrmion is oriented parallel or antiparallel to the vortex, and $\lambda_{vs} \simeq 0.8\lambda$ (see Ref. [23] and the Supplemental Material [46]). For $d_I = 0$, this potential could also represent qualitatively the effect of proximity-induced SOC between the SC and CM layers [20,22].

Mean-field theory.—We analyze the stability of the homogeneous phase using a nonlocal mean-field approach, where the free energy (1) is expressed as a functional of the densities coarse grained over many intervortex and interskyrmion spacings [57], $\bar{\mathcal{F}}_{\rm int}[n_v, n_s] = \frac{1}{2}\sum_{\alpha,\beta}\int d^2\boldsymbol{r}d^2\boldsymbol{r}' n_\alpha(\boldsymbol{r})n_\beta(\boldsymbol{r}')V_{\alpha\beta}(\boldsymbol{r}-\boldsymbol{r}')$, where $\alpha, \beta = v, s$, with the constraints $\int d^2\boldsymbol{r} n_\alpha(\boldsymbol{r}) = N_\alpha$. The homogeneous distributions of vortices and skyrmions, $n_{v0} = N_v/A$ and $n_{s0} = N_s/A$, are a trivial solution of the minimization of this functional.

To evaluate the stability with respect to density fluctuations at specific wave vectors $\boldsymbol{k}$, we rewrite $\bar{\mathcal{F}}_{\rm int}$ as a functional in Fourier space,

$$\bar{\mathcal{F}}[\tilde{n}_v, \tilde{n}_s] = \mathcal{F}_0 + \frac{1}{2}\sum_{\alpha,\beta}\int \frac{d^2\boldsymbol{k}}{4\pi^2}\tilde{n}_\alpha(-\boldsymbol{k})\tilde{n}_\beta(\boldsymbol{k})\tilde{V}_{\alpha\beta}(k), \qquad (2)$$

where $\tilde{f}(\boldsymbol{k}) = \int d^2\boldsymbol{r} f(\boldsymbol{r})e^{-i\boldsymbol{k}\cdot\boldsymbol{r}}$. Stability requires that the Hessian matrix $\mathcal{D}_{\alpha\beta}(\boldsymbol{k}) = [\delta^2\bar{\mathcal{F}}_{\rm int}/\delta\tilde{n}_\alpha(-\boldsymbol{k})\delta\tilde{n}_\beta(\boldsymbol{k})] = \tilde{V}_{\alpha\beta}(k)$ be positive definite, i.e., $\det\mathcal{D}_{\alpha\beta}(\boldsymbol{k}) = \tilde{V}_{vv}(k)\tilde{V}_{ss}(k) - \tilde{V}_{vs}(k)^2 > 0$, for all $\boldsymbol{k}$. However, this condition can be violated at a single nonzero wave number k_*, satisfying the conditions

$$[\det\mathcal{D}_{\alpha\beta}(k)]_* = 0, \qquad \left[\frac{d}{dk}\det\mathcal{D}_{\alpha\beta}(k)\right]_* = 0, \qquad (3)$$

where the subscript $*$ means evaluation at k_*. The first equation establishes a simple relation between the energy scales at the stability boundary,

$$|\epsilon_{vs}| = \gamma_*\sqrt{\epsilon_{vv}\epsilon_{ss}}, \qquad (4)$$

where $\gamma_* = \sqrt{\tilde{v}_{vv}(k_*)\tilde{v}_{ss}(k_*)}/\tilde{v}_{vs}(k_*)$ is a dimensionless constant, with $\tilde{v}_{\alpha\beta} \equiv \tilde{V}_{\alpha\beta}/\epsilon_{\alpha\beta}$. In other words, the homogeneous phase breaks down when $|\epsilon_{vs}| > \gamma_*\sqrt{\epsilon_{vv}\epsilon_{ss}}$, irrespective of whether the vortex-skyrmion interaction is attractive or repulsive, as long as a nonzero solution for k_* exists. The combination of both conditions in (3) leads to an implicit equation relating k_* to all three length scales,

$$\left[\frac{\tilde{v}'_{vv}}{\tilde{v}_{vv}} + \frac{\tilde{v}'_{ss}}{\tilde{v}_{ss}} - 2\frac{\tilde{v}'_{vs}}{\tilde{v}_{vs}}\right]_* = 0, \qquad (5)$$

where the prime means derivative with respect to k. This general result can be applied to other models of the interaction potentials. For the specific model considered here, $\tilde{v}_{vv} = 2\pi/(k^2 + k/\Lambda)$, $\tilde{v}_{ss} = 2\pi/(k^2 + \xi_s^{-2})$, and $\tilde{v}_{vs} = \pi\lambda_{vs}^3 k K_1(k\lambda_{vs})$, and Eq. (5) reads

$$\frac{2k_* + \Lambda^{-1}}{k_*(k_* + \Lambda^{-1})} + \frac{2k_*}{k_*^2 + \xi_s^{-2}} = 2\lambda_{vs}\frac{K_0(k_*\lambda_{vs})}{K_1(k_*\lambda_{vs})}. \qquad (6)$$

Note that the left-hand side of this equation decreases monotonically toward zero, while the right-hand side increases monotonically toward $2\lambda_{vs}$. Therefore, no matter the combination of values of the length scales Λ, ξ_s, and

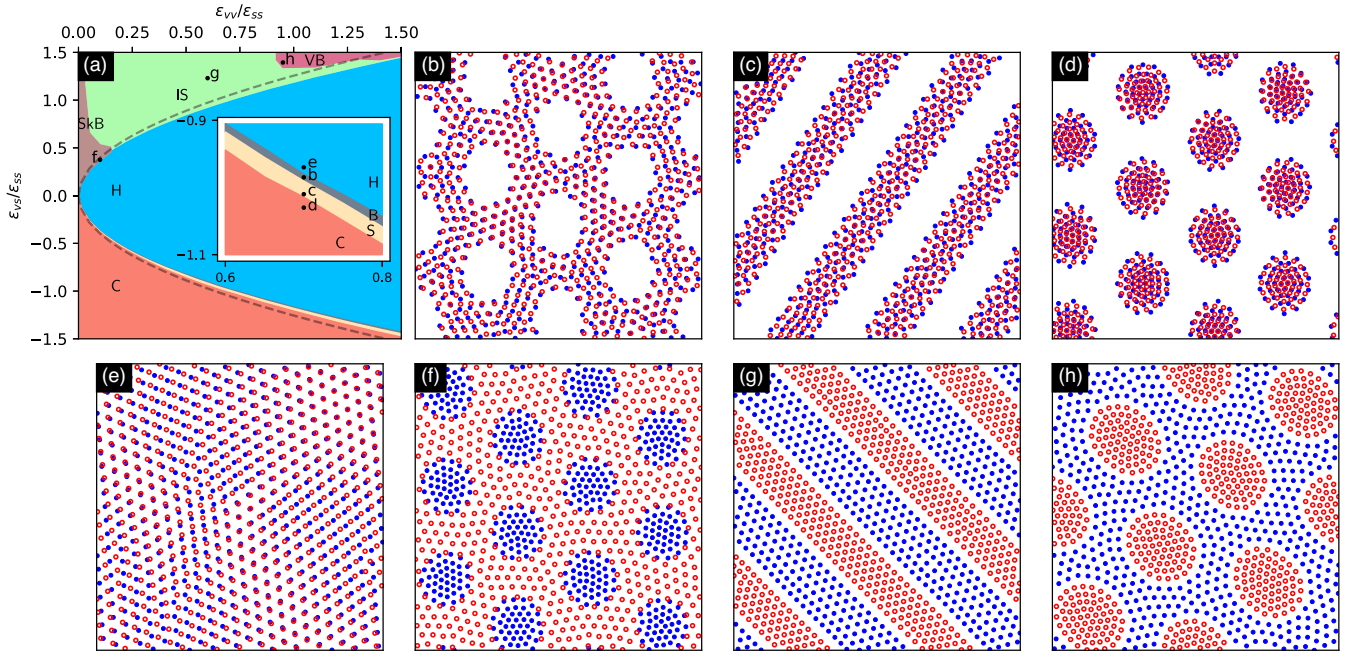

FIG. 2. Phase diagram (a) of the composite skyrmion-vortex system for $n_{v0} = 3.55\lambda_{vs}^{-2}$, $n_{s0} = 3.77\lambda_{vs}^{-2}$, and $\xi_s = 0.5\lambda_{vs}$, featuring the homogeneous phase (H) and six distinct microphases: bubbles (B), stripes (S), clusters (C), vortex-filled skyrmion bubbles (SkB), intercalated stripes (IS), and skyrmion-filled vortex bubbles (VBs). The dashed line is the theoretical stability boundary of the homogeneous phase calculated from Eqs. (4) and (6). Inset: enlarged phase diagram for better identification of phases B and S. (b)–(h) Representative configurations of vortices (blue dots) and skyrmions (red rings) for each phase as indicated in (a).

λ_{vs}, there is always a single nonzero solution for k_*. Upon fulfillment of condition (4), the homogeneous state becomes unstable with respect to density fluctuations of wavelength $2\pi/k_*$.

Numerical simulations.—To investigate further the structure of the modulated phases and analyze the phase boundaries beyond mean-field approximation, we introduce coupled Langevin equations of motion for vortices and skyrmions,

$$\eta_v \frac{d\boldsymbol{r}_{vi}}{dt} = -\frac{\delta \mathcal{F}_{\rm int}}{\delta \boldsymbol{r}_{vi}} + \boldsymbol{\gamma}_{vi}(t), \tag{7}$$

$$(\eta_s + \boldsymbol{G}\times)\frac{d\boldsymbol{r}_{si}}{dt} = -\frac{\delta \mathcal{F}_{\rm int}}{\delta \boldsymbol{r}_{si}} + \boldsymbol{\gamma}_{si}(t), \tag{8}$$

where η_v (η_s) is the vortex (skyrmion) viscous drag coefficient and $\boldsymbol{G} = G\hat{\boldsymbol{z}}$ is the gyromagnetic vector [23]. The Gaussian noises $\boldsymbol{\gamma}_{vi}(t)$ and $\boldsymbol{\gamma}_{si}(t)$ satisfy $\langle \gamma^{\mu}_{\alpha i}(t)\rangle = 0$ and $\langle \gamma^{\mu}_{\alpha i}(t)\gamma^{\nu}_{\alpha j}(t')\rangle = \Gamma_{\alpha}\delta_{\mu\nu}\delta_{ij}\delta(t-t')$, where $\mu, \nu = x,\ y$ and $\alpha = v,\ s$. In thermal equilibrium, $\Gamma_{\alpha} = 2\eta_{\alpha}k_BT$ [53,58]. For the purpose of minimizing the full free energy (1), we set arbitrarily $\eta_v = \eta_s$ and $G = 0$ and integrate Eqs. (7) and (8) on a square simulation box of side L with periodic boundary conditions, while slowly reducing the noise amplitude. Further simulation details and a discussion about the effect of η_v, η_s, and G on the relaxation toward equilibrium are given in the Supplemental Material [46].

For a general view of the possible phases, we minimize the free energy (1) for $N_v = 512$ and $N_s = 544$, $L = 12\lambda_{vs} = 9.6\lambda$, and $\xi_s = 0.5\lambda_{vs}$, thoroughly exploring the parameter space defined by ϵ_{vv} and ϵ_{vs}, treated as independent variables. The resulting phase diagram is shown in Fig. 2. Notice that the boundary of the homogeneous H phase lies close to the theoretical instability line, Eq. (4), and is perfectly symmetric with respect to the sign of ϵ_{vs}. Within this boundary (small $|\epsilon_{vs}|$), both vortices and skyrmions form homogeneous and slightly distorted triangular lattices [46]. For larger $|\epsilon_{vs}|$, the homogeneous phase gives place to surprisingly diverse microphases. For attractive skyrmion-vortex potential ($\epsilon_{vs} < 0$), we observed a narrow region of vortex-skyrmion bubble lattices B in the vicinity of the H-phase boundary, followed by commensurate stripes S, and then commensurate cluster lattices C, which ultimately dominate the large $|\epsilon_{vs}|$ region of the phase diagram. In contrast, for repulsive skyrmion-vortex potential ($\epsilon_{vs} > 0$), the switching between the different microphases is strongly dependent on the ratio $\epsilon_{vv}/\epsilon_{ss}$. For large (small) $\epsilon_{vv}/\epsilon_{ss}$, the vortex (skyrmion) lattice becomes stiffer, forcing skyrmions (vortices) to form compact clusters within vortex (skyrmion) bubbles. For intermediate $\epsilon_{vv}/\epsilon_{ss}$, vortices and skyrmions come to terms and form intercalated stripes.

Going beyond the validity limit of the mean-field approximation, we performed a series of simulations for other skyrmion densities, down to $n_{s0} = 0.89\lambda_{vs}^{-2} = 0.22\xi_s^{-2}$. The

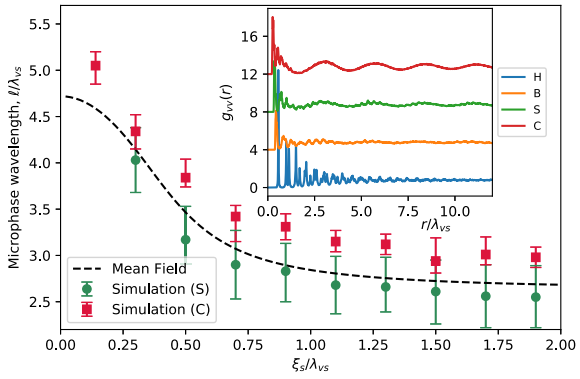

FIG. 3. Wavelength of the stripe and cluster phases simulated for different ξ_s. Here, $L = 24\lambda_{vs}$, $N_v = N_s = 2048$, $\epsilon_{vs} = \epsilon_{ss}$, and ϵ_{vv} is chosen to keep close to the instability line. The full line corresponds to the critical wavelength $2\pi/k_*$, calculated from Eq. (6). Inset: radial vortex-vortex correlation function $g_{vv}(r)$ of configurations representative of the H, B, S, and C phases. The arrows indicate the microphase wavelength of the respective configuration.

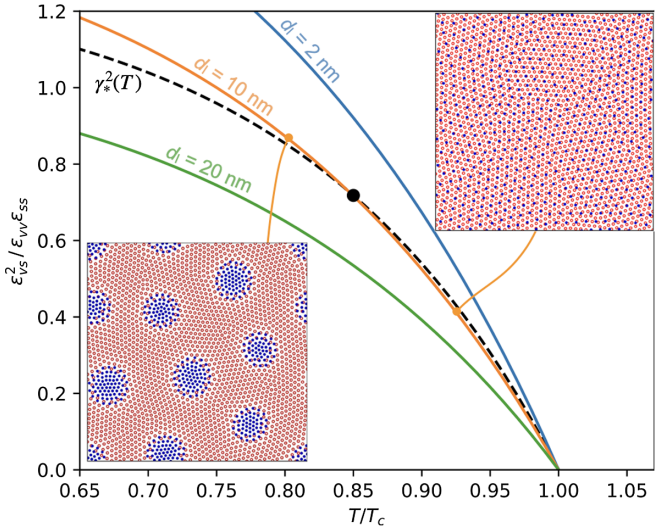

FIG. 4. Temperature dependence of $\gamma^2 = \epsilon_{vs}^2/\epsilon_{vv}\epsilon_{ss}$ calculated for a superconductor-insulator-ferromagnet trilayer considering three different values of d_I. Also shown is the instability line $\gamma_*^2(T)$ (dashes). When $\gamma > \gamma_*$ the homogeneous phase decays to a microphase. The insets are field-cooled vortex-skyrmion configurations for $d_I = 10$ nm at $T_1 = 0.80T_c$ and $T_2 = 0.925T_c$.

results, presented in the Supplemental Material [46], demonstrate that the microphases occupy a larger region of the phase diagram for lower n_{s0}, so that Eq. (9) can be viewed as an upper-limit estimate of the breakdown of the homogeneous phase.

The structure of the microphases is revealed as smooth mesoscale oscillations in the radial correlation function of skyrmions and vortices, $g_{\alpha\alpha}(r)$, a quantity readily accessible in, e.g., neutron diffraction experiments. Here, we use $g_{vv}(r)$ for an accurate estimate of the typical wavelength of the microphases in the vicinity of the instability line as a function of ξ_s (see Fig. 3). To minimize finite size effects, we performed simulations on a large simulation box of size $L = 24\lambda_{vs}$ for $N_v = N_s = 2048$. For each ξ_s, we fixed $\epsilon_{vs} = 1.0\epsilon_{ss}$ and chose ϵ_{vv} in a way to stay close to the boundary of the homogeneous phase. As seen in Fig. 4, the numerical data lie remarkably close to the critical wavelength $\ell_* = 2\pi/k_*$, suggesting that the structure of the microphases is determined precisely by the wave number of the density fluctuations responsible for the breakdown of the homogeneous phase.

Experimental accessibility.—To evaluate the experimental accessibility of the vortex-skyrmion microphases, it is necessary to determine the temperature dependence of the several quantities involved. To be specific, we consider systems comprising a low-T_c superconducting film and a chiral magnetic multilayer with Curie temperature $T_C \gg T_c$. In this case, the operating temperature satisfies $T < T_c \ll T_C$, in which case ξ_s and ϵ_{ss} are essentially constant [59]. In contrast, λ, ϵ_{vv}, and ϵ_{vs} are strongly temperature dependent. In particular, close to the superconducting critical temperature T_c, $\epsilon_{vv}, \epsilon_{vs} \sim 1/\lambda^2(T)$ and thereby $\gamma^2 = \epsilon_{vs}^2/(\epsilon_{vv}\epsilon_{ss}) \sim 1/\lambda^2(T)$ (see Supplemental Material [46]). In this limit, one also has $\Lambda(T) \gg \lambda_{vs}(T) \gg \xi_s$ and Eq. (6) can be considerably simplified leading to $\gamma_*^2 \simeq 15.76\xi_s^2/\lambda^2(T)$. Therefore, for T close to T_c, γ, and γ_* have the same temperature dependence and the condition for vortex-skyrmion microphase reduces to $\gamma_*^2(0) < \gamma^2(0)$ or

$$15.76\frac{\xi_s^2}{\lambda^2(0)} < \frac{\epsilon_{vs}^2(0)}{\epsilon_{vv}(0)\epsilon_{ss}} \sim \frac{\pi}{15}\frac{\xi_s^4(d_S\mathcal{R}_1 + R_{\rm sk}\mathcal{R}_2)^2}{\ell_{\rm ex}^2\lambda^2(0)d_M d_S}. \qquad (9)$$

The right-hand side is a rough estimate of $\gamma^2(0)$ for small skyrmion radius, $\mathcal{R}_1$ and $\mathcal{R}_2$ are dimensionless geometric factors, and $\ell_{\rm ex} = \sqrt{2A/\mu_0 M_s^2}$ is the exchange length of the CM layer, with M_s its saturation magnetization [46]. Away from the $T \to T_c$ limit, the scaling $\gamma, \gamma_* \sim \lambda^{-2}$ is no longer valid and the temperature dependence of each of these quantities has to be determined numerically [46].

For a concrete example, we consider three CM-SC heterostructures identical to each other except for the thickness of their insulating layer: $d_I = 2$, 10, and 20 nm. For the SC layer, we take $d_S = 20$ nm and $\lambda(T) = \lambda(0)/\sqrt{1-(T/T_c)^4}$, with $\lambda(0) = 150$ nm. For the CM layer, we choose $d_M = 10$ nm, $R_{\rm sk} = 40$ nm, $\xi_s = 50$ nm, $A = 10.45$ pJ/m, and $M_s = 1.0$ MA/m, typical of chiral magnetic multilayers [25,26]. This amounts to $\epsilon_{vv}(0) = 0.482$ aJ and $\epsilon_{ss} = 2.57$ aJ. The vortex-skyrmion coupling constant ϵ_{vs} was computed as a function of temperature for each d_I [46]. Notice that the estimated threshold magnetization for skyrmion-induced vortex-antivortex pairs in the SC layer is [21] $M_{\rm th} = \phi_0 \ln(\Lambda/2\xi)/(0.86\pi^2\mu_0 d_M R_{\rm sk}) = 2.63$ MA/m $> M_s$, for $T = 0$, $d_I = 0$, and assuming $\xi(0) = 5$ nm for the

superconducting coherence length. Hence vortex-antivortex pairs induced by the skyrmions can be ruled out in this example. In Fig. 4, we plot the ratio $\gamma^2 = \epsilon_{vs}^2/(\epsilon_{vv}\epsilon_{ss})$ as a function of reduced temperature T/T_c for all three samples and the instability line $\gamma_*^2(T)$. For small d_I, the homogeneous phase is unstable as soon as the SC film enters the superconducting state, while for large d_I, the homogeneous phase is stable in the full temperature range of the superconducting state. Interestingly, for the intermediate case $d_I = 10$ nm, $\gamma(T)$ crosses the critical line at $T_* = 0.85T_c$: the system is homogeneous at high temperatures, but breaks down into a modulated phase at $T < T_*$. We further support these results with numerical simulations of $N_v = 512$ and $N_s = 2048$ on a square simulation box of size $L = 2.0$ μm, thus corresponding to an external magnetic field $B = 265$ mT. For all three values of d_I, we simulate field cooling processes from the normal state down to the target temperatures $T_1 = 0.80T_c$ and $T_2 = 0.925T_c$ by first initializing the skyrmions as a triangular lattice (previously annealed in the absence of vortices) and placing the vortices at random positions. From this point on, the binary system is allowed to relax toward a stationary state at the target temperature. The stationary vortex-skyrmion configurations obtained were found to be modulated at both T_1 and T_2 for $d_I = 2$ nm, modulated at T_1 and homogeneous at T_2 for $d_I = 10$ nm, and homogeneous at both temperatures for $d_I = 20$ nm, thus in excellent agreement with the mean-field prediction.

Summary.—In conclusion, we have demonstrated that a binary magnetic skyrmion-superconducting vortex system can exhibit emergent density-modulated phases when the coupling between the superconductor and the ferromagnet is strong enough. For moderate to high skyrmion and vortex densities, the numerical simulations are in excellent agreement with the analytical results for the instability boundary of the homogeneous phase and wavelength of the density modulations, calculated from mean-field density functional theory. We also derived an approximate inequality that allows one to tune material and geometrical parameters for the observation of vortex-skyrmion mesophases. In particular, for intermediate separations between the superconductor and the chiral magnet, it is possible to tune between homogeneous and microphase vortex-skyrmion configurations by changing the temperature of the system. These findings shed light on the general problem of pattern formation in binary mixtures and provide new insights on composite vortex-skyrmion systems, which can be useful for future spintronics and quantum computing applications.

We are grateful to M. M. Milosevic and R. M. Menezes for useful discussions. This work was supported by the Brazilian Agencies FACEPE, under Grant No. APQ-0198-1.05/14, CAPES, and CNPq.

*clecio.cssilva@ufpe.br

[1] H. Yang, S.-H. Yang, S. Takahashi, S. Maekawa, and S. S. Parkin, Extremely long quasiparticle spin lifetimes in superconducting aluminium using mgo tunnel spin injectors, Nat. Mater. **9**, 586 (2010).
[2] J. Linder and J. W. Robinson, Superconducting spintronics, Nat. Phys. **11**, 307 (2015).
[3] M. Eschrig, Spin-polarized supercurrents for spintronics: A review of current progress, Rep. Prog. Phys. **78**, 104501 (2015).
[4] S. Takahashi, H. Imamura, and S. Maekawa, Spin Imbalance and Magnetoresistance in Ferromagnet/Superconductor/Ferromagnet Double Tunnel Junctions, Phys. Rev. Lett. **82**, 3911 (1999).
[5] G.-X. Miao, A. V. Ramos, and J. S. Moodera, Infinite Magnetoresistance from the Spin Dependent Proximity Effect in Symmetry Driven bcc–Fe/V/Fe Heteroepitaxial Superconducting Spin Valves, Phys. Rev. Lett. **101**, 137001 (2008).
[6] B. Li, N. Roschewsky, B. A. Assaf, M. Eich, M. Epstein-Martin, D. Heiman, M. Münzenberg, and J. S. Moodera, Superconducting Spin Switch with Infinite Magnetoresistance Induced by an Internal Exchange Field, Phys. Rev. Lett. **110**, 097001 (2013).
[7] T. Yamashita, K. Tanikawa, S. Takahashi, and S. Maekawa, Superconducting π Qubit with a Ferromagnetic Josephson Junction, Phys. Rev. Lett. **95**, 097001 (2005).
[8] A. Feofanov, V. Oboznov, V. Bol'Ginov, J. Lisenfeld, S. Poletto, V. Ryazanov, A. Rossolenko, M. Khabipov, D. Balashov, A. Zorin *et al.*, Implementation of superconductor/ferromagnet/superconductor π-shifters in superconducting digital and quantum circuits, Nat. Phys. **6**, 593 (2010).
[9] T. Golod, O. M. Kapran, and V. M. Krasnov, Planar Superconductor-Ferromagnet-Superconductor Josephson Junctions as Scanning-Probe Sensors, Phys. Rev. Applied **11**, 014062 (2019).
[10] M. Lange, M. J. Van Bael, Y. Bruynseraede, and V. V. Moshchalkov, Nanoengineered Magnetic-Field-Induced Superconductivity, Phys. Rev. Lett. **90**, 197006 (2003).
[11] M. V. Milošević and F. M. Peeters, Vortex-Antivortex Lattices in Superconducting Films with Magnetic Pinning Arrays, Phys. Rev. Lett. **93**, 267006 (2004).
[12] C. C. de Souza Silva, A. V. Silhanek, J. Van de Vondel, W. Gillijns, V. Metlushko, B. Ilic, and V. V. Moshchalkov, Dipole-Induced Vortex Ratchets in Superconducting Films with Arrays of Micromagnets, Phys. Rev. Lett. **98**, 117005 (2007).
[13] V. Vlasko-Vlasov, U. Welp, G. Karapetrov, V. Novosad, D. Rosenmann, M. Iavarone, A. Belkin, and W.-K. Kwok, Guiding superconducting vortices with magnetic domain walls, Phys. Rev. B **77**, 134518 (2008).
[14] M. Vélez, J. Martín, J. Villegas, A. Hoffmann, E. González, J. Vicent, and I. K. Schuller, Superconducting vortex pinning with artificial magnetic nanostructures, J. Magn. Magn. Mater. **320**, 2547 (2008).
[15] A. Y. Aladyshkin, A. V. Silhanek, W. Gillijns, and V. V. Moshchalkov, Nucleation of superconductivity and vortex matter in superconductor–ferromagnet hybrids, Supercond. Sci. Technol. **22**, 053001 (2009).

[16] Z. Adamus, M. Z. Cieplak, M. Kończykowski, L. Y. Zhu, and C. L. Chien, Influence of magnetic domain landscape on the flux dynamics in superconductor/ferromagnet bilayers, Phys. Rev. B **93**, 054509 (2016).
[17] V. K. Vlasko-Vlasov, F. Colauto, A. I. Buzdin, D. Rosenmann, T. Benseman, and W.-K. Kwok, Manipulating Abrikosov vortices with soft magnetic stripes, Phys. Rev. B **95**, 174514 (2017).
[18] Y.-L. Wang, X. Ma, J. Xu, Z.-L. Xiao, A. Snezhko, R. Divan, L. E. Ocola, J. E. Pearson, B. Janko, and W.-K. Kwok, Switchable geometric frustration in an artificial-spin-ice–superconductor heterosystem, Nat. Nanotechnol. **13**, 560 (2018).
[19] Y.-Y. Lyu, X. Ma, J. Xu, Y.-L. Wang, Z.-L. Xiao, S. Dong, B. Janko, H. Wang, R. Divan, J. E. Pearson *et al.*, Reconfigurable pinwheel artificial-spin-ice and superconductor hybrid device, Nano Lett. **20**, 8933 (2020).
[20] K. M. D. Hals, M. Schecter, and M. S. Rudner, Composite Topological Excitations in Ferromagnet-Superconductor Heterostructures, Phys. Rev. Lett. **117**, 017001 (2016).
[21] S. M. Dahir, A. F. Volkov, and I. M. Eremin, Interaction of Skyrmions and Pearl Vortices in Superconductor-Chiral Ferromagnet Heterostructures, Phys. Rev. Lett. **122**, 097001 (2019).
[22] J. Baumard, J. Cayssol, F. S. Bergeret, and A. Buzdin, Generation of a superconducting vortex via Néel skyrmions, Phys. Rev. B **99**, 014511 (2019).
[23] R. M. Menezes, J. F. S. Neto, Clecio C. de Souza Silva, and M. V. Milošević, Manipulation of magnetic skyrmions by superconducting vortices in ferromagnet-superconductor heterostructures, Phys. Rev. B **100**, 014431 (2019).
[24] S. Rex, I. V. Gornyi, and A. D. Mirlin, Majorana bound states in magnetic skyrmions imposed onto a superconductor, Phys. Rev. B **100**, 064504 (2019).
[25] X. Palermo, N. Reyren, S. Mesoraca, A. V. Samokhvalov, S. Collin, F. Godel, A. Sander, K. Bouzehouane, J. Santamaria, V. Cros, A. I. Buzdin, and J. E. Villegas, Tailored Flux Pinning in Superconductor-Ferromagnet Multilayers with Engineered Magnetic Domain Morphology from Stripes to Skyrmions, Phys. Rev. Applied **13**, 014043 (2020).
[26] A. P. Petrović, M. Raju, X. Y. Tee, A. Louat, I. Maggio-Aprile, R. M. Menezes, M. J. Wyszyński, N. K. Duong, M. Reznikov, C. Renner, M. V. Milošević, and C. Panagopoulos, Skyrmion-(anti)Vortex Coupling in a Chiral Magnet-Superconductor Heterostructure, Phys. Rev. Lett. **126**, 117205 (2021).
[27] E. S. Andriyakhina and I. S. Burmistrov, Interaction of a Néel-type skyrmion with a superconducting vortex, Phys. Rev. B **103**, 174519 (2021).
[28] G. Yang, P. Stano, J. Klinovaja, and D. Loss, Majorana bound states in magnetic skyrmions, Phys. Rev. B **93**, 224505 (2016).
[29] E. Mascot, J. Bedow, M. Graham, S. Rachel, and D. K. Morr, Topological superconductivity in skyrmion lattices, npj Quantum Mater. **6**, 6 (2021).
[30] F. S. Bates and G. H. Fredrickson, Block copolymers-designer soft materials, Phys. Today **52**, No. 2, 32 (1999).
[31] S. Krishnamoorthy, C. Hinderling, and H. Heinzelmann, Nanoscale patterning with block copolymers, Mater. Today **9**, 40 (2006).
[32] Y. Zhuang, K. Zhang, and P. Charbonneau, Equilibrium Phase Behavior of a Continuous-Space Microphase Former, Phys. Rev. Lett. **116**, 098301 (2016).
[33] A. Stradner, H. Sedgwick, F. Cardinaux, W. C. Poon, S. U. Egelhaaf, and P. Schurtenberger, Equilibrium cluster formation in concentrated protein solutions and colloids, Nature (London) **432**, 492 (2004).
[34] N. Osterman, D. Babič, I. Poberaj, J. Dobnikar, and P. Ziherl, Observation of Condensed Phases of Quasiplanar Core-Softened Colloids, Phys. Rev. Lett. **99**, 248301 (2007).
[35] N. Tasios, S. Samin, R. van Roij, and M. Dijkstra, Microphase Separation in Oil-Water Mixtures Containing Hydrophilic and Hydrophobic Ions, Phys. Rev. Lett. **119**, 218001 (2017).
[36] G. Malescio and G. Pellicane, Stripe phases from isotropic repulsive interactions, Nat. Mater. **2**, 97 (2003).
[37] C. J. Olson Reichhardt, C. Reichhardt, and A. R. Bishop, Structural transitions, melting, and intermediate phases for stripe- and clump-forming systems, Phys. Rev. E **82**, 041502 (2010).
[38] H. J. Zhao, V. R. Misko, and F. M. Peeters, Analysis of pattern formation in systems with competing range interactions, New J. Phys. **14**, 063032 (2012).
[39] C. N. Varney, K. A. H. Sellin, Q.-Z. Wang, H. Fangohr, and E. Babaev, Hierarchical structure formation in layered superconducting systems with multi-scale inter-vortex interactions, J. Phys. Condens. Matter **25**, 415702 (2013).
[40] L. Komendová, M. V. Milošević, and F. M. Peeters, Soft vortex matter in a type-i/type-ii superconducting bilayer, Phys. Rev. B **88**, 094515 (2013).
[41] S. Zhang, J. Zhang, Q. Zhang, C. Barton, V. Neu, Y. Zhao, Z. Hou, Y. Wen, C. Gong, O. Kazakova *et al.*, Direct writing of room temperature and zero field skyrmion lattices by a scanning local magnetic field, Appl. Phys. Lett. **112**, 132405 (2018).
[42] N. K. Duong, M. Raju, A. Petrović, R. Tomasello, G. Finocchio, and C. Panagopoulos, Stabilizing zero-field skyrmions in Ir/Fe/Co/Pt thin film multilayers by magnetic history control, Appl. Phys. Lett. **114**, 072401 (2019).
[43] S. Meyer, M. Perini, S. von Malottki, A. Kubetzka, R. Wiesendanger, K. von Bergmann, and S. Heinze, Isolated zero field sub-10 nm skyrmions in ultrathin co films, Nat. Commun. **10**, 1 (2019).
[44] J. Brandão, D. Dugato, R. Seeger, J. Denardin, T. Mori, and J. Cezar, Observation of magnetic skyrmions in unpatterned symmetric multilayers at room temperature and zero magnetic field, Sci. Rep. **9**, 1 (2019).
[45] Y. Guang, I. Bykova, Y. Liu, G. Yu, E. Goering, M. Weigand, J. Gräfe, S. K. Kim, J. Zhang, H. Zhang *et al.*, Creating zero-field skyrmions in exchange-biased multilayers through x-ray illumination, Nat. Commun. **11**, 949 (2020).
[46] See Supplemental Material at http://link.aps.org/supplemental/10.1103/PhysRevLett.128.057001 for additional data, details of the simulation procedure, and calculation of the skyrmion-vortex coupling energy, which also includes Refs. [47–51].
[47] P. Chaikin and T. Lubensky, *Principles of Condensed Matter Physics* (Cambridge University Press, Cambridge, England, 2000).

[48] N. Romming, A. Kubetzka, C. Hanneken, K. von Bergmann, and R. Wiesendanger, Field-Dependent Size and Shape of Single Magnetic Skyrmions, Phys. Rev. Lett. **114**, 177203 (2015).

[49] G. Carneiro and E. H. Brandt, Vortex lines in films: Fields and interactions, Phys. Rev. B **61**, 6370 (2000).

[50] I. S. Gradshteyn and I. M. Ryzhik, *Table of Integrals, Series, and Products*, 7th ed. (Elsevier/Academic Press, Amsterdam, 2007).

[51] A. Vansteenkiste, J. Leliaert, M. Dvornik, M. Helsen, F. Garcia-Sanchez, and B. Van Waeyenberge, The design and verification of MuMax3, AIP Adv. **4**, 107133 (2014).

[52] E. H. Brandt, Vortex-vortex interaction in thin superconducting films, Phys. Rev. B **79**, 134526 (2009).

[53] S.-Z. Lin, C. Reichhardt, C. D. Batista, and A. Saxena, Particle model for skyrmions in metallic chiral magnets: Dynamics, pinning, and creep, Phys. Rev. B **87**, 214419 (2013).

[54] D. Foster, C. Kind, P. J. Ackerman, J.-S. B. Tai, M. R. Dennis, and I. I. Smalyukh, Composite skyrmion bags in two-dimensional materials, arXiv:1806.02576.

[55] R. Brearton, G. van der Laan, and T. Hesjedal, Magnetic skyrmion interactions in the micromagnetic framework, Phys. Rev. B **101**, 134422 (2020).

[56] D. Capic, D. A. Garanin, and E. M. Chudnovsky, Skyrmion–skyrmion interaction in a magnetic film, J. Phys. Condens. Matter **32**, 415803 (2020).

[57] This approach is expected to be accurate when the mean spacing between particles of the same species is smaller than the relevant characteristic lengths of the interactions, that is, when $a_v \equiv n_v^{-1/2} \lesssim \Lambda$, λ_{vs} and $a_s \equiv n_s^{-1/2} \lesssim \xi_s$, λ_{vs}.

[58] S. A. Trugman and S. Doniach, Vortex dynamics in inhomogeneous superconducting films, Phys. Rev. B **26**, 3682 (1982).

[59] R. Tomasello, K. Y. Guslienko, M. Ricci, A. Giordano, J. Barker, M. Carpentieri, O. Chubykalo-Fesenko, and G. Finocchio, Origin of temperature and field dependence of magnetic skyrmion size in ultrathin nanodots, Phys. Rev. B **97**, 060402(R) (2018).